ACS chemical biology

Articles

pubs.acs.org/acschemicalbiology

Targeting GSK3 from *Ustilago maydis*: Type-II Kinase Inhibitors as Potential Antifungals

Christian Grütter,[†] Jeffrey R. Simard,[‡] Svenja C. Mayer-Wrangowski,[†] Peter H. Schreier,[§,∥] José Pérez-Martín,[⊥] André Richters,[†,‡] Matthäus Getlik,[‡] Oliver Gutbrod,[§] Christoph A. Braun,[§] Michael E. Beck,[§] and Daniel Rauh*[,†,‡]

[†]Fakultät Chemie - Chemische Biologie, Technische Universität Dortmund, Otto-Hahn-Strasse 6, D-44227 Dortmund, Germany

[‡]Chemical Genomics Centre of the Max Planck Society, Otto-Hahn-Strasse 15, D-44227 Dortmund, Germany

[§]Bayer CropScience AG, Alfred-Nobel-Strasse 50, D-40789 Monheim am Rhein, Germany

[∥]Institute for Genetics, University of Cologne, Zülpicher Strasse 47a, D-50674 Cologne, Germany

[⊥]Institute of Functional Biology and Genomics, CSIC, 37007 Salamanca, Spain

Supporting Information

ABSTRACT: Protein kinases are key enzymes in the complex regulation of cellular processes in almost all living organisms. For this reason, protein kinases represent attractive targets to stop the growth of eukaryotic pathogens such as protozoa and fungi. However, using kinase inhibitors to fight against these organisms bears several challenges since most of them are unselective and will also affect crucial host kinases. Here we present the X-ray structure of glycogen synthase kinase 3 from the fungal plant pathogen *Ustilago maydis* (*Um*GSK3) and its inhibition by type-II kinase inhibitors. Despite the high sequence homology between the human and the fungal variant of this vital kinase, we found substantial differences in the conformational plasticity of their active sites. Compounds that induced such conformational changes could be used to selectively inhibit the fungal kinase. This study serves as an example of how species-specific selectivity of inhibitors can be achieved by identifying and addressing the inactive state of a protein kinase. In addition to this, our study gives interesting insights into the molecular plasticity of *Um*GSK3 by revealing a previously unknown inactive conformation of this important kinase family.

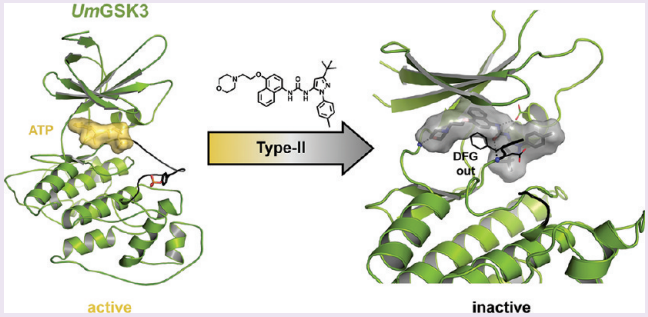

Protein kinases are key players in many cellular signaling processes. The dysregulation of kinase activity can have significant effects on vital physiological functions and hence the well-being of an organism. Therefore, they represent important drug targets, and a lot of effort has been put into the development of kinase inhibitors by both academia and the pharmaceutical industry over the past decades. Consequently, a multitude of kinase inhibitors with different modes of action have been developed to date. In contrast to this, the use of kinase inhibitors as potential agents to fight human or plant pathogenic organisms such as protozoa[1] or fungi[2,3] has been investigated only to a marginal extent.

Recently, a number of research studies have described the development of novel antimicrobial agents by targeting eukaryotic protein kinases,[4,5] indicating a growing interest in such approaches. This trend is further stimulated by the increase in knowledge about eukaryotic signaling pathways (*e.g.*, through the adaptation of novel kinase perturbation strategies[6]) and the availability of the genome sequence data of numerous parasites, which in turn led to the identification of pathogen relevant protein kinases and their validation as drug targets. Unfortunately, the development of potent kinase inhibitors as antiparasitic or antifungal agents is very challenging. These inhibitors usually suffer from a poor selectivity, since they bind to the highly conserved nucleotide binding cleft of the kinase domain, thereby targeting many other kinases, including those of the host organism. For some kinases it has been shown that it is possible to create selective ATP competitive inhibitors,[7,8] but this approach remains very labor intensive.

A more promising strategy to develop selective kinase inhibitors is to identify molecules that bind to less conserved regions outside or in close proximity of the nucleotide binding cleft and are able to alter specific molecular activation and deactivation mechanisms. Compounds from this category are (i) type-II and type-III kinase inhibitors that stabilize an enzymatically inactive state of the kinase domain in which the DFG motif and the following activation loop adopt a closed conformation (also known as the DFG-out conformation)[9] and (ii) type-IV kinase inhibitors that bind far away from the catalytic site and stabilize an arrangement of regulatory domains

Received: March 19, 2012
Accepted: April 30, 2012
Published: April 30, 2012

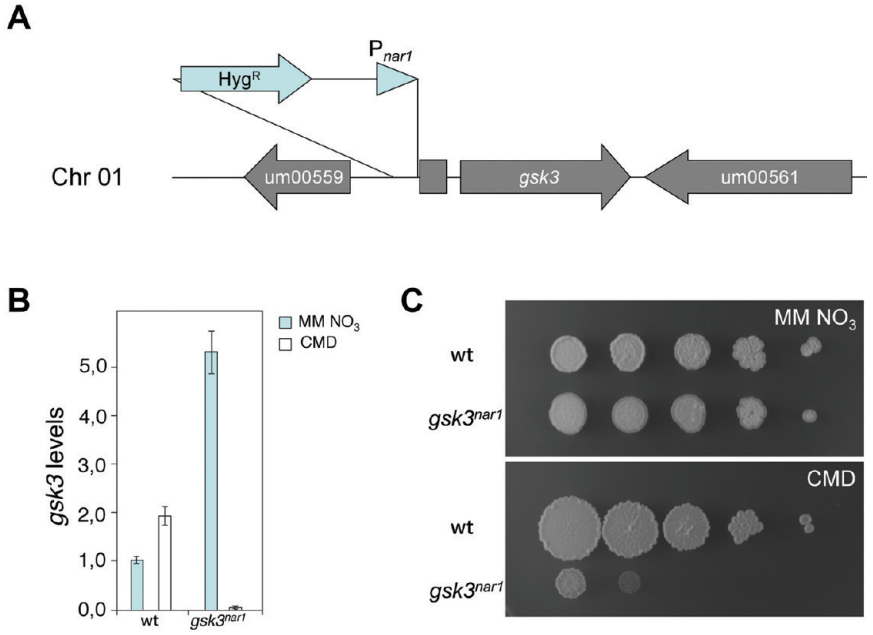

Figure 1. Conditional down-regulation of GSK3 impairs growth in *Ustilago maydis*. (A) Scheme of the conditional allele *gsk3*^{nar1}. A cassette containing the *nar1* promoter as well as an antibiotic (hygromicin) resistance gene was inserted upstream of the start codon of *gsk3*. (B) Levels of *gsk3* mRNA in the conditional strain are shown. The *Ustilago maydis* wild type strain (wt) and the conditional *gsk3*^{nar1} strain were grown for 8 h in permissive (minimal medium with nitrate, MM NO_3) or restrictive conditions (complete medium, CMD). The RNA was extracted and analyzed using RT-PCR. (C) Growth of conditional strain in solid medium. Serial 10-fold dilutions of wild type (wt) and conditional *gsk3*^{nar1} strain cultures were spotted in solid MM NO_3 and CMD. Plates were incubated for 3 days at 28 °C.

that inactivate the catalytic function of the kinase, as observed for Abl[10] or AKT.[11] Nevertheless, there is only a limited amount of information available about the conformational plasticity of protein kinases that would facilitate the straightforward design of such ligands. This is especially the case for protein kinases from relatively uncharacterized eukaryotic pathogens. Thus, the identification of such inhibitors remains a challenging task.

The identification of GSK3 from the parasitic fungus *Ustilago maydis* as one of the kinase targets of N-substituted diaminopyrimidines,[5] a compound class that inhibits the growth of *U. maydis*, aroused our interest to identify novel inhibitors for *Um*GSK3. Moreover, GSK3 is also a known drug target in other eukaryotic pathogens (*e.g.*, *Trypanosoma brucei*[12]), suggesting that the identification of potent inhibitors of this kinase would open the door to such an "indication shift". A vast plethora of GSK3 inhibitors of diverse chemotypes and modes of action have been developed over the past decades,[13,14] but so far there are no type-II/III kinase inhibitors known that would inhibit this kinase by stabilizing an inactive conformation.

To improve the chances of finding *Um*GSK3 inhibitors that do not affect the human homologue *Hs*GSK3β, we focused our search on type-II/III kinase inhibitors. In this paper, we describe the outcome of this approach as well as the detailed structural and biochemical evaluation of GSK3 from *Ustilago maydis*.

RESULTS AND DISCUSSION

Target Validation and Inhibitor Screening. To evaluate the functional relevance of GSK3 in *Ustilago maydis*, we first prepared a haploid *Ustilago* strain in which the GSK3 protein can be conditionally depleted. This was achieved through the implementation of the *nar1* promoter of *Ustilago maydis*, which is induced when the cells are grown in the presence of nitrate ions and strongly repressed in medium containing ammonium ions as the nitrogen source.[15] We constructed a chimeric allele (*gsk3*^{nar1}) by fusing the *nar1* promoter to the coding region of *gsk3* and replacing the native allele with the conditional allele (Figure 1A). When these *nar1* mutant cells were incubated under restrictive conditions (CMD), we could observe a strong decrease of the *gsk3* mRNA levels (Figure 1B). In contrast to this, the *gsk3* mRNA levels were 5-fold higher than the wild-type control at permissive conditions (MM NO_3), indicating that the introduction of the nitrogen source-regulated *nar1* promoter was successful. We could observe a strong decrease in growth for the *gsk3*^{nar1} *Ustilago* strain on ammonium-containing solid medium (CMD) when compared to wild-type *Ustilago*, whereas on minimal nitrate medium (MM NO_3) both strains grew equally well (Figure 1C). This result shows that *Ustilago maydis* requires GSK3 activity for survival. Inhibition of *Um*GSK3 by small molecules should therefore result in the death of the fungus.

Because almost all known potent inhibitors of GSK3 are ATP competitive and therefore rather unselective, we decided to screen for potential allosteric modulators (type-II and type-III) hoping to find a way to inhibit *Um*GSK3 in a novel and more selective way. For this purpose, we performed a pilot screen with an in-house compound library containing different types (I–IV) of protein kinase inhibitors[16−18] including several potent type-II/type-III kinase inhibitors of p38α or cSrc kinases.[19,20] We utilized the activity-based Z'Lyte kinase assay[21] to allow the robust and fast determination of the inhibitory potency of the selected compounds against *Um*GSK3. Besides several strong type-I inhibitors, *e.g.*, PIK-75 (**1**) and compound **2**, we found that some type-II kinase inhibitors were able to reduce the kinase activity of *Um*GSK3 significantly (Figure 2). BIRB-796 (**3**) and sorafenib (**4**) showed the strongest effect

dx.doi.org/10.1021/cb300128b | *ACS Chem. Biol.* 2012, 7, 1257−1267

A

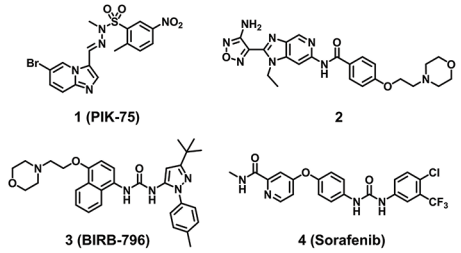

Compound	IC_{50} *Um*GSK3	$\frac{IC_{50}^{25\ Km}}{IC_{50}^{Km}}$	$\frac{IC_{50}^{t=0}}{IC_{50}^{t=60}}$	IC_{50} *Hs*GSK3β
1	0.008 ± 0.002	5.6	0.8	0.010 ± 0.005
2	0.35 ± 0.10	5.4	1.1	0.42 ± 0.17
3	1.06 ± 0.25	1.0	7.6	37*)
4	0.71 ± 0.21	1.9	7.0	8.3 ± 0.8

B

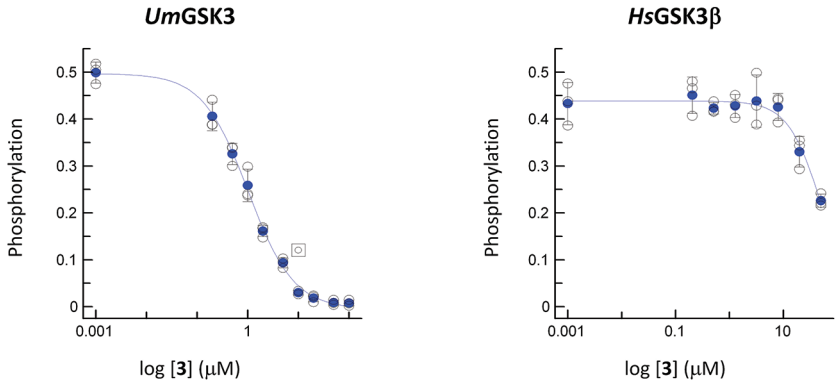

Figure 2. Inhibition of *Um*GSK3 by kinase inhibitors. (A) Structures of the four most potent hits from a pilot screen using a small focused compound library containing all different types of kinase inhibitors. Inhibition data for *Um*GSK3 and *Hs*GSK3*β* are summarized in the table. IC_{50} values are given in *μ*M. "$IC_{50}^{25\ Km}/IC_{50}^{Km}$" represents the ratio of two independent IC_{50} measurements at ATP Km and at 25× ATP Km, here referred to as the "ATP competitive score". "$IC_{50}^{t=0}/IC_{50}^{t=60}$" represents the ratio of two independent IC_{50} measurements with no preincubation time (t = 0) and with 60 min preincubation time, here referred to as the "slow binder score". The IC_{50} values marked with an asterisk (*) were extrapolated from an incomplete dose–response curve. (B) Enzyme activities of *Um*GSK3 and *Hs*GSK3*β* plotted against increasing concentrations of BIRB-796 (**3**). The dose–response curves reveal potent inhibition of *Um*GSK3 but not *Hs*GSK3*β* by this type-II kinase inhibitor.

with IC_{50}'s of 1 and 0.7 *μ*M, respectively. This result was somewhat unexpected, since the human and other investigated GSK3 homologues are not known to adopt an inactive conformation that can be efficiently targeted by these types of inhibitors.[22] Indeed, when the same compounds were tested against *Hs*GSK3*β*, inhibition experiments revealed a more than 10-fold weaker inhibition (**4**) or no inhibition (**3**) (Figure 2).

To further explore the inhibition properties of **3** and **4** toward *Um*GSK3, we performed additional kinetic studies using the activity-based Omnia assay,[23] which allows the direct monitoring of kinase phosphorylation reactions over time. This assay platform allowed us to examine the inhibition efficiency of these compounds in the presence of different ATP concentrations as well as their time-dependent binding behavior (Figure 2A). We determined an "ATP competitive score" by taking the ratio of IC_{50} measurements at ATP Km and at 25× ATP Km (ATP competitive score = $IC_{50}^{25\ Km}/IC_{50}^{Km}$). Additionally, we determined a "slow binder score" by taking the ratio of IC_{50} measurements with inhibitor preincubation times of 0 and 60 min (slow binder score = $IC_{50}^{t=0}/IC_{50}^{t=60}$). These scores contain information related to the k_{off} rates and k_{on} rates of a given inhibitor. We found that the inhibition of *Um*GSK3 by BIRB-796 (**3**) and sorafenib (**4**) clearly depends on the preincubation time (slow binder score = 7.6, 7.0). No preincubation resulted in much higher IC_{50} values, indicating that these inhibitors possess relatively slow k_{on} rates. For long preincubation times (*e.g.*, 60 min), the determined IC_{50} values are lower and only weakly ATP-dependent (ATP competitive score = 1.0, 1.9). This shift in IC_{50} is far less than predicted by the Cheng–Prusoff equation for ATP competitive inhibitors. Obviously, BIRB-796 (**3**) and sorafenib (**4**) have also exceptionally slow k_{off} rates resulting in extended inhibitor residence times within the kinase active site. In other words, they are only weakly affected by varying ATP concentrations once bound to the kinase. Such a slow binding behavior is a strong indication for ligand-induced conformational changes of the kinase domain, a prominent characteristic of type-II binding inhibitors. Apparently, BIRB-796 (**3**) and sorafenib (**4**) are able to lock the kinase in an inactive conformation in contrast to two other tested screening hits, PIK-75 (**1**) and **2**, which are known ATP competitive kinase inhibitors, which did not show this effect.

Structural Characterization of *Um*GSK3. The fact that *Um*GSK3 but not *Hs*GSK3*β* can be potently inhibited by type-II kinase inhibitors, in combination with the observed slow binding kinetics, clearly indicates that there are substantial differences in the activation loop mobility between these two kinases. For *Hs*GSK3*β*, we have never observed any time-dependent inhibition behavior (slow k_{on} or k_{off} rates) that would imply larger conformational changes upon ligand binding. This finding is rather surprising since their catalytic sites (including the activation loop) share a sequence identity of almost 90%. To determine if this difference in the conformational plasticity can be explained on a molecular level, we set out to crystallize *Um*GSK3 and designed several crystallization constructs (Figure 3A) with the help of a *Um*GSK3 homology model based on two published crystal structures of *Hs*GSK3*β* (PDB IDs: 1I09 and 1PYX) (Figure 3B).

dx.doi.org/10.1021/cb300128b | *ACS Chem. Biol.* 2012, 7, 1257–1267

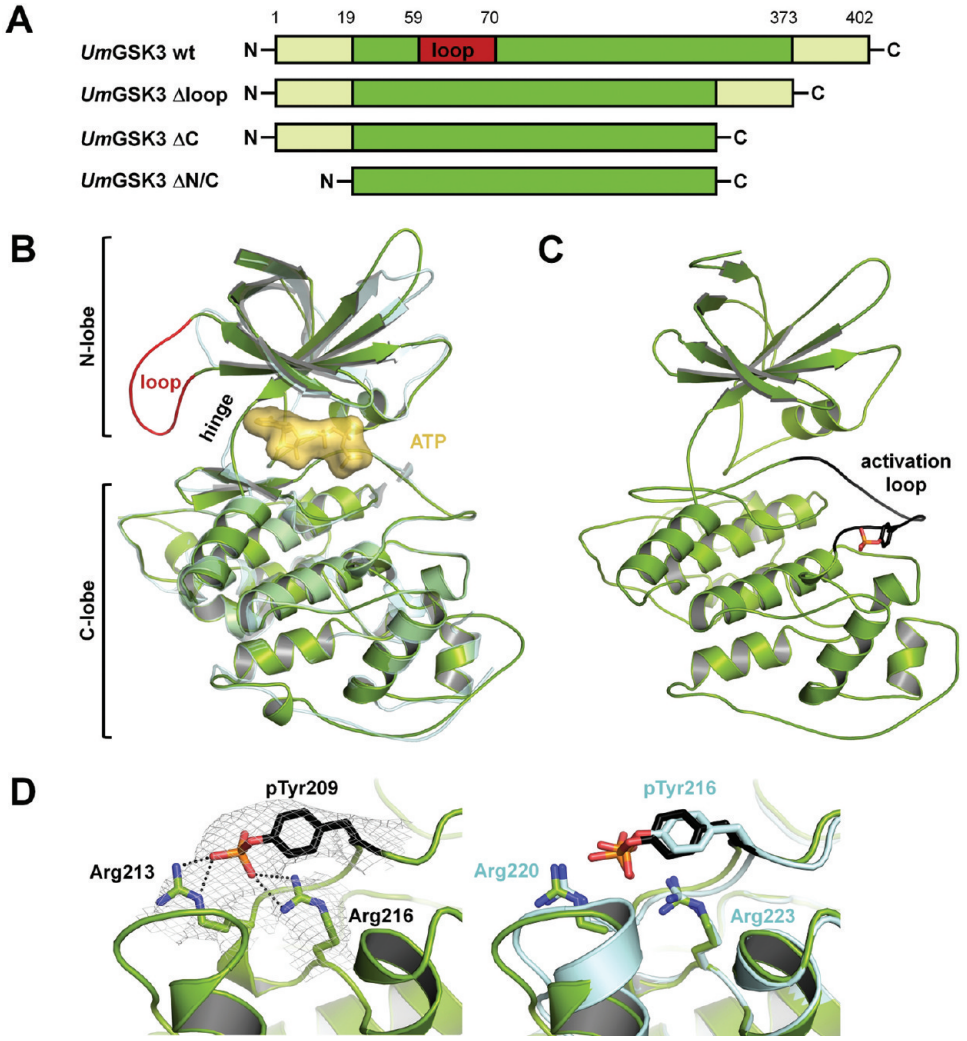

Figure 3. Expression constructs and overall structure of *Um*GSK3 Δloop. (A) Four *Um*GSK3 constructs were designed and tested for expression and crystallization trials. *Um*GSK3 wt: wild-type kinase, *Um*GSK3 Δloop: loop deletion mutant, *Um*GSK3 ΔC and *Um*GSK3 ΔC/N: two constructs additionally lacking the C- or the N- and C-terminal part. Only the first two constructs could be obtained from *E. coli* in soluble form. (B) A homology model of *Um*GSK3 (green) superimposed with a crystal structure of *Hs*GSK3*β* (blue, PDB ID: 1I09) highlighting the differences between the two kinases. This analysis was used as basis for construct design. Red: Additional loop segment of *Um*GSK3. Yellow: ATP bound to the ATP binding pocket. (C) Cartoon representation of the overall structure of *Um*GSK3 Δloop containing a phosphorylated Tyr209 (shown as black sticks), which represents an autophosphorylation site commonly found in GSK3-like kinases. The activation loop is marked in black. (D) Detailed view of the close environment of pTyr209 including the experimental electron density map (2fo−fc) contoured at 1σ. The two side chains of Arg213 and Arg216 (green sticks) form salt bridges with the phosphate group attached to Tyr209. Right: A comparison of pTyr209 (black) with Tyr216-phosphorylation found in human GSK3*β* (blue; PDB ID: 1GNG).

We constructed three shorter *Um*GSK3 constructs lacking potentially disordered regions by shortening the C-terminus (*Um*GSK3 ΔC) or both termini (*Um*GSK3 ΔC/N)[24] and by deleting an additional loop segment of about 12 amino acids in length located preceding the glycine rich loop within the N-lobe of the kinase (*Um*GSK3 Δloop). Aside from the wild-type kinase, only the loop deletion construct could be expressed and purified in soluble form from *E. coli*, whereas the N- and C-terminal shortened constructs exhibited a strong aggregation tendency and could not be used for crystallization.

After extensive crystallization attempts, we obtained hexagonal shaped crystals for the *Um*GSK3 Δloop construct. The crystals belong to the trigonal space group $P32_1$ and possess a high solvent content of about 75%, resulting in a Matthews Coefficient (V_M)[25] of 5.0. From one of these single crystals, we collected a data set to a resolution of 3.3 Å at the Swiss Light Source in Villigen (PSI, Switzerland), which enabled us to solve the structure by molecular replacement using a known *Hs*GSK3*β* structure (PDB ID: 1I09) as template (Figure 3C). Together with the recently published structure of GSK3 from the pathogenic protozoa *Leishmania major* (PDB ID: 3E3P) and a putative uncharacterized protein from *Cryptosporidium parvum iowa ii* (PDB ID: 3EB0), these represent the only structural studies of non-human glycogen synthase kinases to date. The final model of the *Um*GSK3 Δloop construct comprises residues 13−375. Tyr195 located within the activation loop is phosphorylated and forms salt bridges with two adjacent arginine residues, Arg199 and Arg202. This residue is homologous to Tyr216 of *Hs*GSK3*β* (see Figure 3D), which is a known autophosphorylation site.[26] This residue is highly conserved in all GSK3-like kinases, and its phosphorylation is required for kinase activity.[27]

Since we found no significant structural differences between the loop deletion mutant of *Um*GSK3 and known *Hs*GSK3*β*

dx.doi.org/10.1021/cb300128b | *ACS Chem. Biol.* 2012, 7, 1257−1267

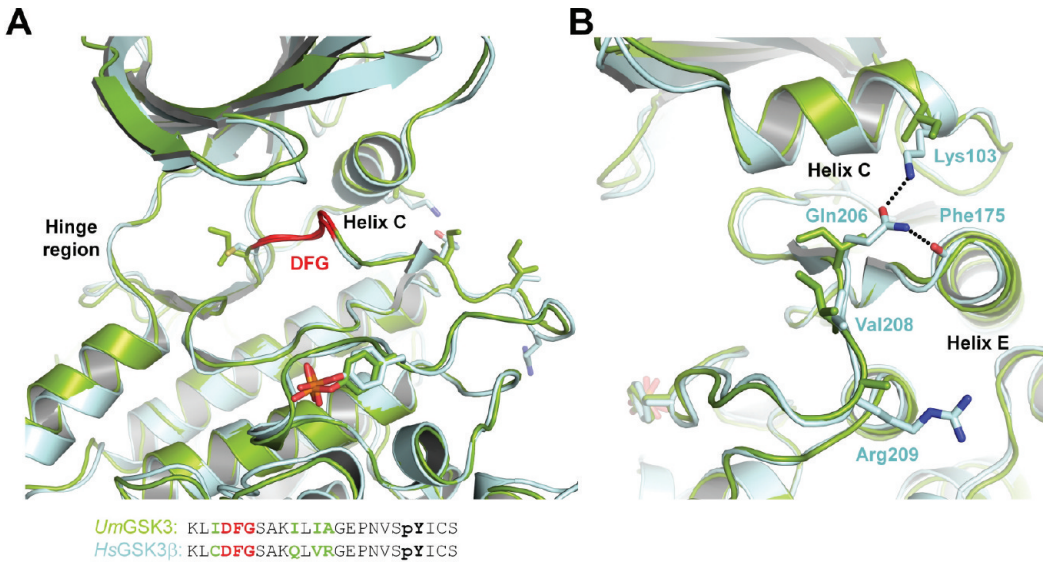

Figure 4. Comparison of the active site of *Um*GSK3 and *Hs*GSK3*β*. (A) Superimposition of the ATP and substrate binding cleft of the human (blue) and fungal (green) GSK3. Residues that are not conserved, indicated by green letters in a sequential alignment of the activation loop segments, are represented as sticks. The DFG motif is marked in red. (B) Detailed view of the interactions which stabilize the activation loop conformation in *Hs*GSK3*β*. The direct hydrogen-bond interactions between Gln206 and two adjacent residues (Lys103 and Phe175) are shown as black dotted lines.

structures, we wondered if the additional loop segment present in the wild-type *Um*GSK3 could explain the observed differences in their molecular plasticity. However, the deletion mutant (*Um*GSK3 Δloop) exhibits almost identical activity, ATP affinity, and inhibition properties compared to the wild-type kinase (data not shown). Thus, deletion of this loop segment has no direct influence on the activation loop mobility *in vitro*.

Comparison with *Hs*GSK3*β*. We compared the catalytic cores of *Um*GSK3 and *Hs*GSK3*β* in detail, which includes the ATP binding site, the glycine-rich loop, as well as the activation loop. Within these regions, there are virtually no significant structural differences. We could identify only four residues that are not conserved between these two kinases (see Figure 4A). One of these residues is located within the ATP binding cleft, and three of them are located on the activation loop, resulting in differences within the hydrogen bonding network that holds the activation loops in an active conformation. Gln206 of *Hs*GSK3*β* seems to be particularly important since it forms two direct hydrogen bonding contacts to the side chain amine of Lys103, located in helix C, and the backbone carbonyl of Phe175 of helix E (see Figure 4B). We hypothesized that this residue functions as a "pin" that helps lock the activation loop in an active conformation, as observed in all GSK3 structures to date. Interestingly, we found that these hydrogen bonds are missing in the fungal homologue due to the presence of an isoleucine residue (Ile185) at this position, resulting in a smaller number of direct hydrogen bonding contacts between the activation loop and the rest of the kinase. We wondered if these additional interactions might be the reason for the differences of the activation loop mobility and prepared a mutant of *Hs*GSK3*β* (GSK3*β* Q206I). Unfortunately this GSK3*β* variant was also poorly inhibited by BIRB-796 (**3**) even at concentrations up to 50 *μ*M and thereby behaved like wild-type GSK3*β*. The same was observed for a triple mutant, where all three amino acids of the activation loop were exchanged (Q206I, V208I, R209A) to generate a *Hs*GSK3*β* kinase with a "fungal" activation loop sequence. These results suggest that the activation loop sequence alone does not explain the differences in sensitivity of these homologues to BIRB-796 (**3**). Thus far, we have been unable to find a convincing explanation on a molecular level for the observed potency differences and activation loop dynamics for both GSK3 variants.

Binding Dynamics of Type-II Kinase Inhibitors. Our preliminary inhibition results and kinetic studies with *Um*GSK3 strongly suggest that *Um*GSK3 is susceptible to the ligand-induced conformation changes associated with the binding of type-II ligands, analogous to other kinases such as cSrc or p38*α*. Unfortunately, we were not able to produce any complex crystal structures that would have served as the ultimate proof of such an inactive conformation in *Um*GSK3. Therefore, we decided to further explore the dynamics of type-II ligand binding using the fluorescence labels in kinases (FLiK) technology, which allows the direct detection of specific conformational changes in kinases.[28,29] On the basis of our *Um*GSK3 structure and a sequence analysis, we designed a FLiK labeling mutant, where a cysteine residue was introduced into the N-terminal region of the activation loop (S184C) right after the DFG motif to enable labeling of the loop with an environmentally sensitive fluorophore, acrylodan. The fluorescently tagged *Um*GSK3 exhibits changes in its fluorescence emission spectra upon addition of kinase inhibitors that cause the tagged activation loop to change conformation (*e.g.*, **3** and **4**) (Figure 5A). This change in emission intensities (*e.g.*, ratio of intensities of two emission maxima) can then be used to plot binding curves in order to determine the K_d of ligand binding (Figure 5B). Labeled *Um*GSK3 was incubated with serially diluted BIRB-796 (**3**) in 384-well plates, and the plate was measured after increasing incubation times, which revealed that the K_d of **3** (~0.8 *μ*M for *Um*GSK3) was time-dependent. More specifically, the K_d decreased 2-fold when measured after incubation times of 20 and 60 min but did not shift further over a period of 24 h. When monitoring the change in acrylodan emission intensity at a single wavelength over time, we found that the addition of 5 *μ*M **3** or **4** to acrylodan-labeled *Um*GSK3 resulted in fluorescence decays that were readily fit to a first-order function. A single dose of **3** bound to *Um*GSK3 with a half-time ($t_{1/2}$) of ~90 s, while an equivalent concentration of **4** bound with a $t_{1/2}$

dx.doi.org/10.1021/cb300128b | *ACS Chem. Biol.* 2012, 7, 1257–1267

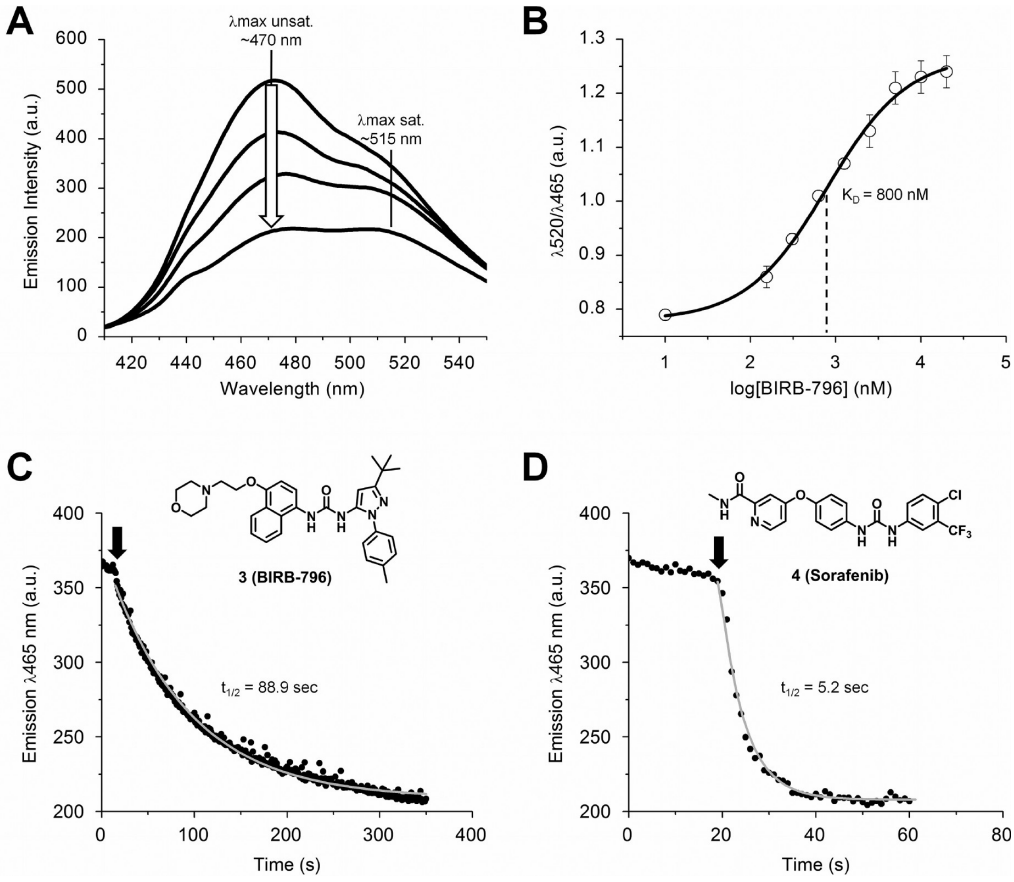

Figure 5. Investigation of the binding mode and binding dynamics of BIRB-796 (**3**) and sorafenib (**4**) using the FLiK technology. (A) Changes in the fluorescence spectra of the *Um*GSK3 FLiK construct upon addition of **3** or **4**. (B) Determination of the K_d value for **3** after 1 h incubation time. (C, D) Kinetic measurements for the binding of both type-II inhibitors showing slow k_{on} rates, revealing a pronounced slow binding behavior caused by conformational rearrangements of the kinase.

of ∼5 s, approximately 10-fold faster (Figure 5C,D). These results fit the trends published elsewhere in which the FLiK technology was applied to human p38α kinase. For p38α, both **3** and **4** bound at even slower rates to the kinase, and the binding of **4** was 100-fold faster than that of **3**.[28] We postulate that the faster kinetics of sorafenib (**4**) are likely a result of its more flexible chemical scaffold, which is less bulky and contains more rotatable bonds, allowing it to more quickly adapt to the DFG-out binding pocket and to change kinase conformation in these kinases.

High-Throughput Screening and Hit Validation. Since the FLiK assay preferentially detects and selects for inhibitors that bind to the inactive conformation of *Um*GSK3, we adapted it to a 384-well format suitable for high-throughput screening. We then screened a kinase focused collection of ∼2000 compounds consisting of type-I/II/III and covalent kinase inhibitors that were either synthesized in our lab or obtained from commercial sources (BioFocus DPI and ChemDiv). In primary screening initiatives, labeled kinase was applied to a single concentration of each compound (10 μM). BIRB-796 (**3**) served as the positive control for the DFG-out conformation, and DMSO served as the negative control. Compounds that induced a fluorescence ratio change of at least 35% of the positive control were selected for follow-up dose−response screens to confirm binding.

The resulting collection of confirmed binders consisted of several "type-II like" scaffolds as well as additional compounds that may have unpredictable or type-I like binding modes. These hits can be roughly divided into 5 classes according to their core structure (Figure 6). The hits were subsequently tested in activity-based assays, and IC_{50} values were determined to confirm their inhibitory potency, which were found to be in the low micromolar to midnanomolar range. In addition, the most potent members of each class were further tested for their "slow binding" character using time- and ATP-dependent inhibition experiments.

Within the class of 1,4-hybrid compounds (**5**−**8**), **5** was the weakest, while **8** showed the best potency with an IC_{50} value of around 1.2 μM as well as a clear time-dependent binding behavior with an ATP competitive score of 2.1. The weak ATP competitive characteristics of this compound class are not as pronounced as for BIRB-796 (**3**), where the IC_{50} values did not vary for different ATP concentrations after a preincubation time of 60 min (IC_{50} 25 Km/IC_{50} Km = 1.0), indicating that the k_{off} rates of **5**−**8** are faster. Nevertheless, their slow binder scores suggest that conformational changes must be involved in the binding process, thereby resulting in slower k_{on} rates. Consistent with these slow binding characteristics, the corresponding IC_{50} values for the *Hs*GSK3β were roughly 10-fold higher than for *Um*GSK3, again demonstrating that *Hs*GSK3β does not readily adopt a DFG-out conformation which can accommodate these types of inhibitors. From a set of thiazolo-ureas (**9**, **10**, and **11**)[30] we could identify a similar binding behavior for compound **9**, with an ATP competitive score of 2.1 and a

dx.doi.org/10.1021/cb300128b | *ACS Chem. Biol.* 2012, 7, 1257−1267

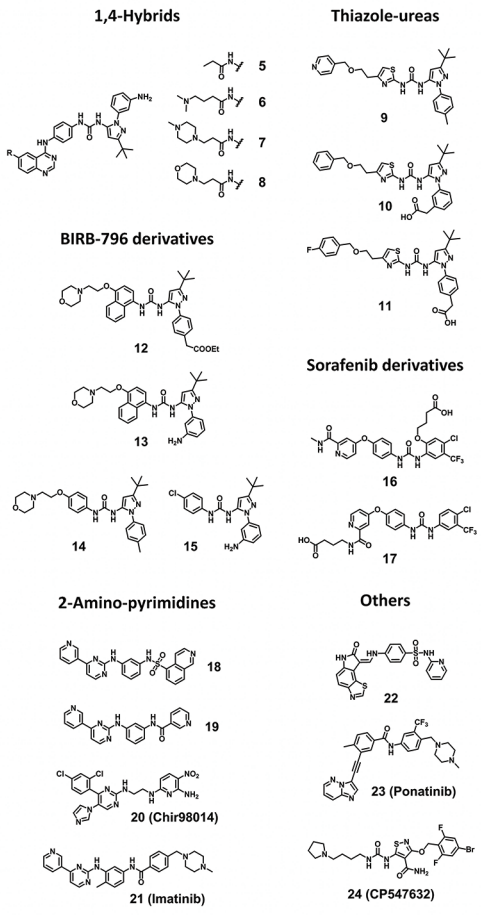

Compound	IC_{50} *Um*GSK3	$\frac{IC_{50}^{25\ Km}}{IC_{50}^{Km}}$	$\frac{IC_{50}^{t=0}}{IC_{50}^{t=60}}$	IC_{50} *Hs*GSK3β
1,4-Hybrids				
5	1.8 ± 1.5	5.9	n.d.	45*)
6	2.4 ± 0.2	3.4	1.2	43*)
7	2.3 ± 0.4	3.9	1.5	29*)
8	1.2 ± 0.6	2.1	2.6	18*)
Thiazole-ureas				
9	2.3 ± 0.9	2.1	3.8	9.6 ± 1.5
10	10.6 ± 0.6			
11	8.5 ± 7.2			
BIRB-796 derivatives				
3	1.06 ± 0.25	1.0	7.6	37*)
12	1.8 ± 0.5	1.8	5.2	>50
13	1.1 ± 0.3	1.4	2.1	>50
14	10.3 ± 5.6	6.9	0.9	>50
15	7.8 ± 2.6	4.0	1.3	>50
Sorafenib derivatives				
4	0.71 ± 0.21	1.9	7.0	8.3 ± 0.8
16	0.057 ± 0.011	1.4	2.9	0.86 ± 0.18
17	0.154 ± 0.103	1.9	2.7	3.3 ± 0.6
2-Amino-pyrimidines				
18	1.14 ± 0.40	8.4	0.8	2.1 ± 0.1
19	3.01 ± 0.56	10.2	1.1	2.4 ± 0.2
20	0.0047 ± 0.0004	7.1	0.9	0.0041 ± 0.0004
21	>50			
Others				
22	2.2 ± 0.3	5.3	0.6	n.d.
23	2.8 ± 2.0	1.2	3.5	12.3 ± 2.8
24	0.054 ± 0.014	8.6	0.6	0.089 ± 0.009

Figure 6. HTS hit validation and inhibitor classification. Chemical structures of 22 strong binders and type-II like kinase inhibitor hits from a FLiK HTS screening campaign with ∼2000 compounds. The hits are divided into six different classes according to their core structures. IC_{50} values for the inhibition of *Um*GSK3 and *Hs*GSK3*β* as well as the ATP competitive and slow binder scores are summarized in the tables next to each compound class. IC_{50} values that were extrapolated from incomplete dose−response curves are marked with an asterisk (*)). N.d.: not determined.

slow binder score of 3.8. The BIRB-796 derivatives **12** and **13** exhibited the most prominent slow binding characteristics. This result was not surprising, since our preliminary kinetic experiments with BIRB-796 (**3**) showed that this type of inhibitor possesses extraordinarily slow k_{on} rates. In contrast to this, **14** and **15**, representing smaller entities of the original BIRB-796 structure, are purely ATP competitive with much lower binding affinities. These inhibition results show a clear structure−activity relationship, revealing that the naphthyl moiety as well as the combination of moieties that bind within the allosteric pocket (pyrazolo-urea moiety) and the hinge region of the ATP site (morpholino moiety) are all essential for the type-II binding character and high affinity of **3** and its derivatives toward *Um*GSK3. Strikingly, the same compounds are either inactive or exhibit only weak inhibition potency for the human homologue.

The sorafenib based hits represent the most interesting compound class. They are fairly potent with IC_{50} values ranging from 60 (**16**) to 700 nM (**4**), exhibit slow binding characteristics (IC_{50} t = 0/IC_{50} t = 60 between 4.9 and 7), and are only weakly affected by changes of the ATP concentration, thus implying slow to moderate k_{on} and k_{off} rates. They also show a species-selective inhibition behavior with 10- to 20-fold higher IC_{50} values for the inhibition of the human homologue. In contrast to this, the 2-amino pyrimidine based compounds **18** and **19** (imatinib like scaffold) and **20** (a potent GSK3 inhibitor developed by Chiron for the treatment of type-II diabetes)[31] inhibit *Um*GSK3 and the *Hs*GSK3*β* with similar potency, indicating a pure ATP competitive binding mode, which was confirmed by their high ATP competitive scores. This also holds true for the other hits (compounds **22**−**24**), which all have varying scaffolds. Although they exhibit moderate (**23** and **24**) to strong (**22**) potencies, they are all purely ATP competitive with the exception of **23**, which was designed to be a type-II kinase inhibitor and turned out to be a slow binder for *Um*GSK3.

In summary we found a total of 7 potent *Um*GSK3 inhibitors from four different type-II compound classes that showed only a moderate to weak inhibitory effect on *Hs*GSK3*β*, and they all exhibit slow binding characteristics, which implies a true DFG-out binding mode. Interestingly, all of these compounds possess a urea scaffold as a central unit, except for ponatinib (**23**). On the basis of the kinetic results and on our knowledge gleaned from previously determined co-crystal structures of cSrc and p38*α* with pyrazolo-urea based type-II and type-III kinase inhibitors, we propose a similar binding mode as observed for the published co-crystal structures of p38*α* with BIRB-796 (PDB ID: 1KV2)[32] or sorafenib (pdb-ID: 3GCS).[28] Therefore we prepared a DFG-out model of *Um*GSK3 using these crystal structures as templates and performed docking studies with BIRB-796 (**3**), sorafenib (**4**), and the potent sorafenib derivatives **16** and **17**. The proposed binding modes for the calculated DFG-out model of

dx.doi.org/10.1021/cb300128b | *ACS Chem. Biol.* 2012, 7, 1257−1267

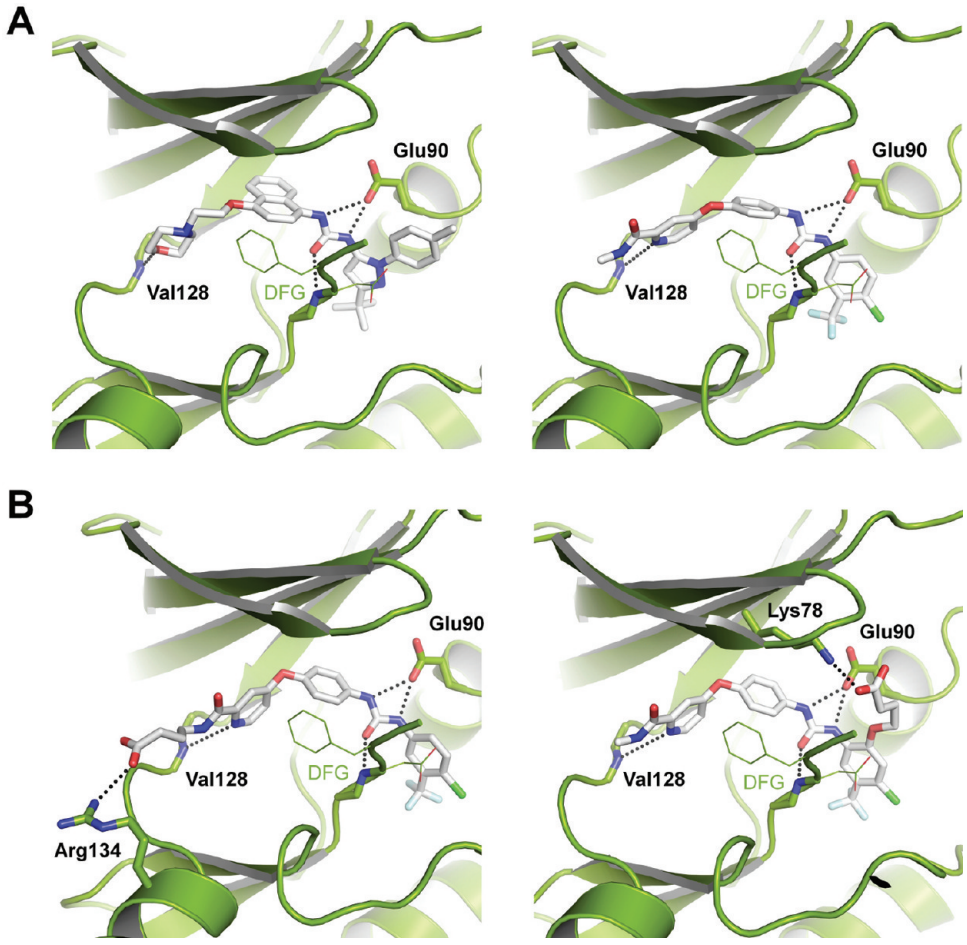

Figure 7. Prediction of the inactive conformation of *Um*GSK3 and the type-II binding modes of BIRB-796 (**3**), sorafenib (**4**), **16**, and **17**. (A) Two figures showing **3** (left) and **4** (right) docked into the ATP binding site of inactive *Um*GSK3. Both compounds exhibit a typical type-II binding mode forming key hydrogen bond interactions with the side chain of Glu90 (from helix C) and the backbone nitrogens of Asp193 (DFG motif) and Val128 (hinge region). (B) Docking results of the two most potent hit compounds **16** (right) and **17** (left). Their extended carboxy side chains allow additional hydrogen bonding interactions with basic amino acids (Arg134, Lys78) that are located in close proximity to the ligands, which might explain their enhanced inhibition potency compared to **4**. The inactive conformation of *Um*GSK3 was modeled based on a crystal structure of p38α in DFG-out conformation (PDB ID: 1KV2).

*Um*GSK3 are shown in Figure 7. We could observe no distorted ligand geometries or clashes with amino acid residues within the *Um*GSK3 binding pocket, indicating that these docking solutions represent reasonable binding scenarios. The overall binding modes of the ligand core structures are typical for this urea based compound class. More interestingly, we found that the carboxylic acid side chains of **16** and **17** allow additional hydrogen bonding interactions with basic amino acids located within or in close proximity to the binding site (Figure 7B). This fact might explain their superior potency when compared to **4** and demonstrates that there is sufficient room for further improvement of these *Um*GSK3 inhibitors.

Growth Inhibition Tests. With the most potent screening hits, **4**, **16**, **17**, and **20**, we performed several growth inhibition tests using the two *Ustilago* species, *U. maydis* and *U. avenae*. The fungi were grown over 2 days under standardized conditions in the presence of different concentrations of these inhibitors. The fungicide Euparen (**25**) and the kinase inhibitor GLJ10588 (**26**)[5] served as positive controls. The results and the estimated ED_{50} values are given in Table 1.

We could observe a clear reduction of the growth of *U. avenae* in the presence of 200 μM sorafenib (65% growth) resulting in an estimated ED_{50} value of 320 μM. The more potent sorafenib derivatives **16** and **17** as well as the highly potent GSK3 inhibitor Chir98014 (**20**) showed no effect. This result can be explained by the presence of polar groups that are attached to these molecules (carboxylic acids or amines), which most likely prevent their diffusion through the fungal cell walls. *U. maydis* is even more robust and was not affected by any of these inhibitors. These growth inhibition tests show that the identified compounds can be active on *Ustilago*, provided that they are able to pass the fungal cell wall.

Conclusions. The identification of *Um*GSK3 as a potential target for antifungal agents opened up the fundamental question of whether this kinase can be inhibited without affecting the human homologue. In order to achieve interspecies selectivity, we left the vast number of known ATP competitive inhibitors aside and focused on type-II/III kinase inhibitor scaffolds, since they generally exhibit an improved selectivity and have advanced pharmacological properties, such as slow dissociation rates, which increase drug-target residence time.[33] The subsequent finding that the GSK3 from *U. maydis* can be potently inhibited by type-II kinase inhibitors was surprising, because this type of inhibition was not previously described for any member of the GSK family to date. Obviously, *Um*GSK3 possesses a certain conformational flexibility enabling this kinase to adopt an inactive conformation, in

dx.doi.org/10.1021/cb300128b | *ACS Chem. Biol.* 2012, 7, 1257–1267

Table 1. Growth Inhibition Test with *U. maydis* and *U. avenae*[a]

Compounds		Estimated ED_{50} in μM	
Name	Structure	*Ustilago avenae*	*Ustilago maydis*
4	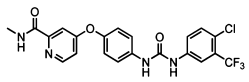	320	n.i.
16	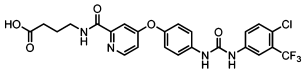	n.i.	n.i.
17	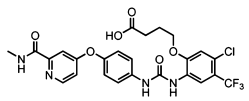	n.i.	n.i.
20	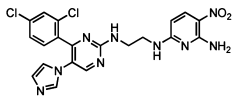	n.i.	n.i.
25	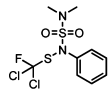	3.2	3.0
26	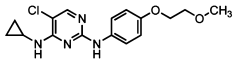	20.0	19.3

[a]n.i: no inhibition.

strict contrast to the human homologue. This fact implies that the regulation of *Um*GSK3 might be substantially different from that of its human counterpart, whose elongated N-terminus is involved in a self-inhibition mechanism.[34] As a further step, the identified inhibitors can now be used to construct a general pharmacophore model for targeting the inactive conformation of *Um*GSK3, which in turn will serve as a valuable starting point for further inhibitor development.

This study demonstrates that it is possible to achieve interspecies-selective inhibition for a given kinase. Within this context, it is important to note that a deeper understanding of the underlying molecular mechanisms of protein kinase regulation is essential for the development of more selective kinase inhibitors. This particularly holds true for the less known protein kinases from eukaryotic pathogens. The investigation of these molecular dynamics will represent one of the future challenges in kinase drug research.

METHODS

Preparation of *Um*GSK3 Constructs. The cDNA of full-length GSK3 (um00560, NCBI accession XP_756707.1) was cloned into pENTR/TEV/D-TOPO vector and subsequently into pDEST17 (both from Invitrogen) according to the manufacturer's instructions. From this vector, the deletion mutants (*Um*GSK3 ΔN, *Um*GSK3 ΔN/C, and *Um*GSK3 Δloop) and the FLiK labeling construct (*Um*GSK3 C41S/C199S/C317S/S184C) were generated by standard PCR cloning strategies. The resulting vectors, encoding the corresponding GSK3 variants with a cleavable hexa-histidine tag at the N-terminus, were transformed into the *E. coli* expression strain BL21(DE3) pLysE. Subsequent expression and purification of the GSK3 constructs was performed as previously described.[5]

Crystallization and Structure Determination of *Um*GSK3 Δloop. Crystallization of *Um*GSK3 Δloop was performed by the hanging drop vapor diffusion method at 277 K in 24-well crystallization plates (Hampton Research) by mixing 1 μL of protein with 1 μL of reservoir solutions containing 8−12% (w/v) EtOH, 1.5 M NaCl, and 40 mM $SrCl_2$ as an additive. Crystals suitable for data collection grew within 5 days. Prior to data collection, crystals were dipped into reservoir buffer containing 25% ethylene glycol as a cryoprotectant and flash frozen in liquid nitrogen. Diffraction data of *Um*GSK3 Δloop were measured at the PX10SA beamline of the Swiss Light Source (PSI, Villingen, Switzerland) using a wavelength close to 1 Å. The data set was processed with XDS and scaled using XSCALE.[35] The *Um*GSK3 Δloop structures were solved by molecular replacement with PHASER[36] using the published *Hs*GSK3*β* structures (PDB ID: 1I09)[37] as template. The molecule in the asymmetric unit was manually modified using the program COOT.[38] The model was first refined with CNS[39] using simulated annealing to reduce model bias. The final refinement was performed with REFMAC5,[40] and the refined structure was validated with PROCHECK.[41] Data collection, structure refinement statistics, PDB ID, and further details for the data collection as well as Ramachandran plot results are shown in Supplementary Table S1. PyMOL[42] was used to produce the figures.

Homology Model Preparation and Docking. The crystal structures of *Um*GSK3 Δloop (PDB ID: 4E7W; residue range 36−319 of chain A) and inactive p38*α* (PDB ID: 1KV2 and 3GCS; residue range 24−308 of chain A) were superimposed and aligned with Strap (STRuctural based Alignment Program; http://3d-alignment.eu). The alignment was manually corrected by taking into account structural information from the structure of *Um*GSK3 Δloop. The final alignment was then fed into the program Modeler 8v2 (http://salilab.org/modeller), using 1KV2[32] and 3GCS[28] as structural templates. 100 models were built using the model building and loop optimization procedures of the program. The resulting models were checked with PROCHECK[41] and further evaluated by visual inspection. The best one was taken as the final model for inactive *Um*GSK3. Docking of BIRB-796 (**3**), sorafenib (**4**), **16**, and **17** was performed using the program Glide of the Schrödinger software suite.

dx.doi.org/10.1021/cb300128b | *ACS Chem. Biol.* 2012, 7, 1257−1267

■ ASSOCIATED CONTENT

Supporting Information

Supplementary table and experimental methods. This material is available free of charge *via* the Internet at http://pubs.acs.org.

Accession Codes

The structure of *Um*GSK3 Δloop was deposited under the PDB accession code 4E7W.

■ AUTHOR INFORMATION

Corresponding Author

*E-mail: daniel.rauh@tu-dortmund.de.

Notes

The authors declare no competing financial interest.

■ ACKNOWLEDGMENTS

J.R.S. was funded by the Alexander von Humboldt Foundation. MSD, Bayer-Schering Pharma, Merck-Serono, and Bayer CropScience are thanked for financial support. The work was supported by the German Federal Ministry for Education and Research through the German National Genome Research Network-Plus (NGFNPlus) (Grant No. BMBF 01GS08104).

■ REFERENCES

(1) Doerig, C. (2004) Protein kinases as targets for anti-parasitic chemotherapy. *Biochim. Biophys. Acta 1697*, 155−168.

(2) Kojima, K., Takano, Y., Yoshimi, A., Tanaka, C., Kikuchi, T., and Okuno, T. (2004) Fungicide activity through activation of a fungal signalling pathway. *Mol. Microbiol. 53*, 1785−1796.

(3) Pillonel, C. (2005) Evaluation of phenylaminopyrimidines as antifungal protein kinase inhibitors. *Pest Manage. Sci. 61*, 1069−1076.

(4) Oduor, R. O., Ojo, K. K., Williams, G. P., Bertelli, F., Mills, J., Maes, L., Pryde, D. C., Parkinson, T., Van Voorhis, W. C., and Holler, T. P. (2011) *Trypanosoma brucei* glycogen synthase kinase-3, a target for anti-trypanosomal drug development: a public-private partnership to identify novel leads. *PLoS Neglected Trop. Dis. 5*, e1017.

(5) Tückmantel, S., Greul, J. N., Janning, P., Brockmeyer, A., Grütter, C., Simard, J. R., Gutbrod, O., Beck, M. E., Tietjen, K., Rauh, D., and Schreier, P. H. (2011) Identification of *Ustilago maydis* aurora kinase as a novel antifungal target. *ACS Chem. Biol. 6*, 926−933.

(6) Koch, A., Rode, H. B., Richters, A., Rauh, D., and Hauf, S. (2012) A chemical genetic approach for covalent inhibition of analogue-sensitive aurora kinase. *ACS Chem. Biol. 7*, 723−731.

(7) Uitdehaag, J. C., Verkaar, F., Alwan, H., de Man, J., Buijsman, R. C., and Zaman, G. J. (2012) A guide to picking the most selective kinase inhibitor tool compounds for pharmacological validation of drug targets. *Br. J. Pharmacol.*, DOI: 10.1111/j.1476-5381.2012.01859.x.

(8) Koeberle, S. C., Romir, J., Fischer, S., Koeberle, A., Schattel, V., Albrecht, W., Grütter, C., Werz, O., Rauh, D., Stehle, T., and Laufer, S. A. (2011) Skepinone-L is a selective p38 mitogen-activated protein kinase inhibitor. *Nat. Chem. Biol. 8*, 141−143.

(9) Rabiller, M., Getlik, M., Klüter, S., Richters, A., Tückmantel, S., Simard, J. R., and Rauh, D. (2010) Proteus in the world of proteins: conformational changes in protein kinases. *Arch. Pharm. 343*, 193−206.

(10) Hantschel, O., Nagar, B., Guettler, S., Kretzschmar, J., Dorey, K., Kuriyan, J., and Superti-Furga, G. (2003) A myristoyl/phosphotyrosine switch regulates c-Abl. *Cell 112*, 845−857.

(11) Wu, W. I., Voegtli, W. C., Sturgis, H. L., Dizon, F. P., Vigers, G. P., and Brandhuber, B. J. (2010) Crystal structure of human AKT1 with an allosteric inhibitor reveals a new mode of kinase inhibition. *PloS One 5*, e12913.

(12) Ojo, K. K., Gillespie, J. R., Riechers, A. J., Napuli, A. J., Verlinde, C. L., Buckner, F. S., Gelb, M. H., Domostoj, M. M., Wells, S. J., Scheer, A., Wells, T. N., and Van Voorhis, W. C. (2008) Glycogen synthase kinase 3 is a potential drug target for African trypanosomiasis therapy. *Antimicrob. Agents Chemother. 52*, 3710−3717.

(13) Martinez, A., Castro, A., Dorronsoro, I., and Alonso, M. (2002) Glycogen synthase kinase 3 (GSK-3) inhibitors as new promising drugs for diabetes, neurodegeneration, cancer, and inflammation. *Med. Res. Rev. 22*, 373−384.

(14) Palomo, V., Soteras, I., Perez, D. I., Perez, C., Gil, C., Campillo, N. E., and Martinez, A. (2011) Exploring the binding sites of glycogen synthase kinase 3. Identification and characterization of allosteric modulation cavities. *J. Med. Chem. 54*, 8461−8470.

(15) Brachmann, A., Weinzierl, G., Kamper, J., and Kahmann, R. (2001) Identification of genes in the bW/bE regulatory cascade in *Ustilago maydis*. *Mol. Microbiol. 42*, 1047−1063.

(16) Pawar, V. G., Sos, M. L., Rode, H. B., Rabiller, M., Heynck, S., van Otterlo, W. A., Thomas, R. K., and Rauh, D. (2010) Synthesis and biological evaluation of 4-anilinoquinolines as potent inhibitors of epidermal growth factor receptor. *J. Med. Chem. 53*, 2892−2901.

(17) Rode, H. B., Sos, M. L., Grütter, C., Heynck, S., Simard, J. R., and Rauh, D. (2011) Synthesis and biological evaluation of 7-substituted-1-(3-bromophenylamino)isoquinoline-4-carbonitriles as inhibitors of myosin light chain kinase and epidermal growth factor receptor. *Bioorg. Med. Chem. 19*, 429−439.

(18) Sos, M. L., Rode, H. B., Heynck, S., Peifer, M., Fischer, F., Klüter, S., Pawar, V. G., Reuter, C., Heuckmann, J. M., Weiss, J., Ruddigkeit, L., Rabiller, M., Koker, M., Simard, J. R., Getlik, M., Yuza, Y., Chen, T. H., Greulich, H., Thomas, R. K., and Rauh, D. (2010) Chemogenomic profiling provides insights into the limited activity of irreversible EGFR Inhibitors in tumor cells expressing the T790M EGFR resistance mutation. *Cancer Res. 70*, 868−874.

(19) Getlik, M., Grütter, C., Simard, J. R., Klüter, S., Rabiller, M., Rode, H. B., Robubi, A., and Rauh, D. (2009) Hybrid compound design to overcome the gatekeeper T338M mutation in cSrc. *J. Med. Chem. 52*, 3915−3926.

(20) Klüter, S., Grütter, C., Naqvi, T., Rabiller, M., Simard, J. R., Pawar, V., Getlik, M., and Rauh, D. (2010) Displacement assay for the detection of stabilizers of inactive kinase conformations. *J. Med. Chem. 53*, 357−367.

(21) Rodems, S. M., Hamman, B. D., Lin, C., Zhao, J., Shah, S., Heidary, D., Makings, L., Stack, J. H., and Pollok, B. A. (2002) A FRET-based assay platform for ultra-high density drug screening of protein kinases and phosphatases. *Assay Drug Dev. Technol. 1*, 9−19.

(22) Anastassiadis, T., Deacon, S. W., Devarajan, K., Ma, H., and Peterson, J. R. (2011) Comprehensive assay of kinase catalytic activity reveals features of kinase inhibitor selectivity. *Nat. Biotechnol. 29*, 1039−1045.

(23) Shults, M. D., Janes, K. A., Lauffenburger, D. A., and Imperiali, B. (2005) A multiplexed homogeneous fluorescence-based assay for protein kinase activity in cell lysates. *Nat. Methods 2*, 277−283.

(24) Mayer-Wrangowski, S. (2010) Cloning, Expression and structural Characterization of a fungal Protein Kinase, Master thesis, Technical University of Dortmund, Dortmund, Germany.

(25) Matthews, B. W. (1968) Solvent content of protein crystals. *J. Mol. Biol. 33*, 491−497.

(26) Cole, A., Frame, S., and Cohen, P. (2004) Further evidence that the tyrosine phosphorylation of glycogen synthase kinase-3 (GSK3) in mammalian cells is an autophosphorylation event. *Biochem.l J. 377*, 249−255.

(27) Hughes, K., Nikolakaki, E., Plyte, S. E., Totty, N. F., and Woodgett, J. R. (1993) Modulation of the glycogen synthase kinase-3 family by tyrosine phosphorylation. *EMBO J. 12*, 803−808.

(28) Simard, J. R., Getlik, M., Grütter, C., Pawar, V., Wulfert, S., Rabiller, M., and Rauh, D. (2009) Development of a fluorescent-tagged kinase assay system for the detection and characterization of allosteric kinase inhibitors. *J. Am. Chem. Soc. 131*, 13286−13296.

(29) Simard, J. R., Klüter, S., Grütter, C., Getlik, M., Rabiller, M., Rode, H. B., and Rauh, D. (2009) A new screening assay for allosteric inhibitors of cSrc. *Nat. Chem. Biol. 5*, 394−396.

(30) Getlik, M., Grütter, C., Simard, J. R., Nguyen, H. D., Robubi, A., Aust, B., van Otterlo, W. A., and Rauh, D. (2012) Structure-based design, synthesis and biological evaluation of N-pyrazole, N'-thiazole urea inhibitors of MAP kinase p38alpha. *Eur. J. Med. Chem. 48*, 1−15.

(31) Cline, G. W., Johnson, K., Regittnig, W., Perret, P., Tozzo, E., Xiao, L., Damico, C., and Shulman, G. I. (2002) Effects of a novel glycogen synthase kinase-3 inhibitor on insulin-stimulated glucose metabolism in Zucker diabetic fatty (fa/fa) rats. *Diabetes 51*, 2903−2910.
(32) Pargellis, C., Tong, L., Churchill, L., Cirillo, P. F., Gilmore, T., Graham, A. G., Grob, P. M., Hickey, E. R., Moss, N., Pav, S., and Regan, J. (2002) Inhibition of p38 MAP kinase by utilizing a novel allosteric binding site. *Nat. Struct. Biol. 9*, 268−272.
(33) Copeland, R. A., Pompliano, D. L., and Meek, T. D. (2006) Drug-target residence time and its implications for lead optimization. *Nat. Rev. Drug Discovery 5*, 730−739.
(34) Dajani, R., Fraser, E., Roe, S. M., Young, N., Good, V., Dale, T. C., and Pearl, L. H. (2001) Crystal structure of glycogen synthase kinase 3 beta: structural basis for phosphate-primed substrate specificity and autoinhibition. *Cell 105*, 721−732.
(35) Kabsch, W. (1993) Automatic processing of rotation diffraction data from crystals of initially unknown symmetry and cell constants. *J. Appl. Crystallogr. 26*, 795−800.
(36) Read, R. J. (2001) Pushing the boundaries of molecular replacement with maximum likelihood. *Acta Crystallogr., Sect. D: Biol. Crystallogr. 57*, 1373−1382.
(37) ter Haar, E., Coll, J. T., Austen, D. A., Hsiao, H. M., Swenson, L., and Jain, J. (2001) Structure of GSK3beta reveals a primed phosphorylation mechanism. *Nat. Struct. Biol. 8*, 593−596.
(38) Emsley, P., and Cowtan, K. (2004) Coot: model-building tools for molecular graphics. *Acta Crystallogr., Sect. D: Biol. Crystallogr. 60*, 2126−2132.
(39) Brünger, A. T., Adams, P. D., Clore, G. M., DeLano, W. L., Gros, P., Grosse-Kunstleve, R. W., Jiang, J. S., Kuszewski, J., Nilges, M., Pannu, N. S., Read, R. J., Rice, L. M., Simonson, T., and Warren, G. L. (1998) Crystallography & NMR system: A new software suite for macromolecular structure determination. *Acta Crystallogr., Sect. D: Biol. Crystallogr. 54*, 905−921.
(40) Murshudov, G. N., Vagin, A. A., and Dodson, E. J. (1997) Refinement of macromolecular structures by the maximum-likelihood method. *Acta Crystallogr., Sect. D: Biol. Crystallogr. 53*, 240−255.
(41) Laskowski, R. A., McArthur, M. W., Moss, D. S., and Thornton, J. M. (1993) PROCHECK: a program to check the stereochemical quality of protein structures. *J. Appl. Crystallogr. 26*, 263−291.
(42) DeLano, W. L. (2002) The PyMOL Molecular Graphics System, http://www.pymol.org.